Journal of Materials Chemistry A

ROYAL SOCIETY OF CHEMISTRY

PAPER

View Article Online
View Journal | View Issue

Cite this: J. Mater. Chem. A, 2022, 10, 18422

Surfactant effects on the synthesis of porous cerium oxide from a type IV deep eutectic solvent†

Iva Manasi, *[a] Mohammad R. Andalibi,[b] Rémi Castaing,[c] Laura Torrente-Murciano [b] and Karen J. Edler *[a]

In this work we present a novel, low temperature and green method for atom-efficient solvothermal synthesis of crystalline, micelle templated cerium IV oxide (ceria) from a type IV deep eutectic solvent (DES) comprising a hydrated cerium containing metal salt, cerium(III) nitrate hexahydrate ($Ce(NO_3)_3 \cdot 6H_2O$), and a hydrogen bond donor, urea, in a molar ratio of 1 : 3.5. Self-assembled nanostructures of ionic and non-ionic surfactants have been recently reported in a cerium nitrate hexahydrate : urea DES [Manasi *et al.*, *J. Chem. Phys.*, 2021, **155**, 084902], which can be exploited to produce nano-templated ceria from these solution. In this work, we have used high concentration (20% w/w) solutions of C-12 and C-16 alkyl chain length cationic surfactants (C_nTAB and C_nTANO$_3$) and C-16 alkyl chain length non-ionic surfactant BrijC_{10} in the DES to alter the porosity of the cerium oxide produced. The characterisation of the cerium oxide has been carried out using SEM/TEM, N_2 sorption, SAXS and TPR to understand and quantify the nature of the crystallinity, morphology and porosity along with CO oxidation for the catalytic activity of the material. The cerium oxide produced by this method has porosity on the 2–5 nm scale and a BET surface area between 40 and 150 $m^2\ g^{-1}$ depending on the amount and type of surfactant. Materials prepared using halide-free cationic surfactants show superior catalytic activity and low activation energies along with high porosity and present potential for improved ceria performance in many industrial applications.

Received 18th July 2022
Accepted 5th August 2022

DOI: 10.1039/d2ta05693c

rsc.li/materials-a

1 Introduction

Cerium IV oxide (CeO_2, ceria) is used in a wide range of applications, *e.g.* auto-exhaust catalysts,[1,2] O_2 permeation membrane systems,[3,4] and electrochromic thin-film applications,[5–7] where the surface properties and porosity of the material can be important. Ceria-based materials are promising candidates both as the support material for the active component(s) or as the catalyst in their own right, in a variety of environmental catalytic applications including CO and NO_x conversion.[8,9] In recent years, research has focused on understanding and manipulating the properties of nanostructured ceria as a way of tuning its redox activity, surface to volume ratio and oxygen storage capacity to improve its performance in various applications. In the past, several strategies have been adopted to achieve low-temperature activity in ceria-based catalysts including doping with transition metals and/or rare earth elements, loading with metals/metal nanoparticles (especially noble metals), and modifying the inherent structural characteristics of ceria.[8–11] Among these methods, modifying the intrinsic structure of ceria is an attractive option, which can be pursued by controlling the synthesis conditions to induce more active (albeit generally less stable) crystallographic planes in the product.[12,13] Additionally, nanosizing and enhancing the specific surface area of ceria samples have been shown to significantly affect their catalytic behaviour.[9,12,14,15]

Various methods have been reported for the synthesis of nanostructured ceria, including combustion syntheses, where "fuels" such as urea or glycine are used in aqueous solutions of cerium nitrate, and heated directly on a hotplate until combustion occurs, causing foaming due to gas evolution.[16–18] These methods produce nanostructured ceria in one step but do not provide controlled structures and are difficult to scale up. Evaporation induced self-assembly methods have also been used to produce gels[19] or particles *via* spray drying,[20] where the incorporation of an organic species such as a surfactant can produce mesoporosity after careful template removal. Hydrothermal and solvothermal methods as reviewed by Sun *et al.*[21] provide more promising avenues for controlled

[a]Department of Chemistry, University of Bath, Claverton Down, Bath, BA2 7AY, UK. E-mail: im554@bath.ac.uk; k.edler@bath.ac.uk; Tel: +44 1225 388388

[b]Department of Chemical Engineering and Biotechnology, West Cambridge Site, Philippa Fawcett Drive, Cambridge, CB3 0AS, UK

[c]Material and Chemical Characterisation Facility, University of Bath, Claverton Down, Bath, BA2 7AY, UK

† Electronic supplementary information (ESI) available: The PXRD peaks, and SEM and TEM images from different ceria samples synthesised from DES without and with added water; exemplar Arrhenius plots over the full CO conversion range from ceria powder; details of the XPS measurements on the different ceria samples. See https://doi.org/10.1039/d2ta05693c

nanoarchitectures. Hydrothermal methods provide many routes for nanostructure modification and morphological control of the ceria produced, *e.g.* varying the reaction time, temperature, urea/base concentration[14,22] and templating using surfactant self-assembly.[23] Porosity modification *via* templating using surfactant self-assembly[24] and microemulsions,[25] or hard templates such as mesoporous silica[26] has been a very popular route in hydrothermal synthesis methods; however, these methods require multiple steps, long reaction times, high temperatures and the use of toxic components. In hydrothermal soft templating methods, the yields can also be quite low due to the decrease in the solubility of the synthesis precursors at high surfactant concentrations.[21] On the other hand, solvothermal methods, reviewed by Walton,[27] provide synthetic and morphology control by direct modification of the solvent environment presenting new exciting opportunities. In this context, deep eutectic solvents (DESs) provide alternative media for solvothermal synthesis applications. DESs are green solvents made by complexation of a (typically ammonium halide and sometimes metal) salt with a hydrogen bond donor, leading to suppression of the melting point at the eutectic ratio.[28]

DESs have low vapour pressure, low flammability, a wide liquid range and a tunable nature. The hydrophobicity and physicochemical properties of a solvent can be altered by changing the salt/hydrogen bond donor or by the addition of various additive compounds, and therefore they have gained interest in a variety of applications from material synthesis[15,29–31] and electroplating[32–34] to pharmaceuticals.[35,36] Organic-based DESs have also been used in the solvothermal synthesis of microporous materials such as metal–organic frameworks or zeolites, where the DES components are incorporated as porogens[37–39] or within the framework of the materials.[40–42] However little work has so far been reported on the use of metal-salt based DES with surfactants as a route to mesoporous inorganic oxide materials.

We reported the first batch synthesis of nanostructured ceria from a widely used DES composed of urea and choline chloride.[15] Recently, we extended this synthesis into flow conditions by employing microreactor technology to intensify the production scheme.[43] The maximum specific surface area of the ceria so-produced was 70–80 $m^2\ g^{-1}$ and attempts to increase this using surfactant templating with sodium dodecylsulphate (SDS) micelles were unsuccessful.[15] In this work, we present the application of a novel type of cerium-based DES for the atom-efficient synthesis of soft-templated high-surface area CeO_2. A halide free type IV DES comprising hydrated salts of lanthanide metals (cerium nitrate, praseodymium nitrate or neodymium nitrate) with urea was reported by Hammond *et al.*[44] The cerium nitrate : urea based DES is used in this solvothermal synthesis, wherein the metal ion acts both as a reactant and as a constituent of the solvent medium. Recent work by our group showed that cationic, anionic and non-ionic surfactants self-assemble in a cerium nitrate : urea mixture, forming micelles,[45] which here are exploited for templating applications in our synthesis of ceria. We compare the porosity and catalytic activity of ceria templated using different micellar templates to demonstrate that by rationally selecting the surfactant, one can obtain a thermally and chemically stable product with distinctly superior low-temperature catalytic activity in the oxidation of CO as a model reaction.

2 Materials and methods

2.1 Materials

Cerium nitrate hexahydrate ($Ce(NO_3)_3 \cdot 6H_2O$; purity 99.5%) was purchased from Acros Organics. Urea (purity ≥99.5%), dodecyl trimethylammonium bromide (C_{12}TAB; purity ≥99%), hexadecyl trimethylammonium bromide (C_{16}TAB; purity ≥99%) and BrijC_{10} ($C_{16}EO_n$, $n \sim 10$) were purchased from Sigma Aldrich, UK. Dodecyl trimethylammonium nitrate ($C_{12}TANO_3$) and hexadecyl trimethylammonium nitrate ($C_{16}TANO_3$) were prepared from C_{12}TAB and C_{16}TAB, respectively, by an ion exchange procedure[46] using Amberlite® IRN78 hydroxide (Acros Organics).

2.2 Sample preparation

$Ce(NO_3)_3 \cdot 6H_2O$: urea DES (Ce : U) was prepared by combining the components in a molar ratio of 1 : 3.5. The mixture was stirred at room temperature until a clear, homogeneous liquid was obtained, which was subsequently sealed and equilibrated overnight. Once formed, the mixture is stable in the liquid state and was used within 2–3 weeks. Surfactant solutions were prepared by mixing 20% w/w C_{12}TAB, C_{16}TAB, BrijC_{10}, $C_{12}TANO_3$ or $C_{16}TANO_3$ in the DES at room temperature until homogeneous mixtures were obtained. DES with added water (DES + 5W) was prepared by mixing the Ce : U DES and water in a molar ratio of 1 : 5 at room temperature until a homogeneous liquid was obtained. Surfactant solutions in DES + 5W were prepared by mixing 20% w/w C_{12}TAB, C_{16}TAB or BrijC_{10} until homogeneous solutions were obtained. To prepare the pastes for the synthesis of metal oxides, the DES or surfactant solutions in DES were weighed (~2 g) into a crucible and heated in a standard laboratory oven at 70 °C for 24 hours. Thereafter, the obtained pastes were placed in a calcination furnace and were heated from ambient to 450 °C at a rate of 5 °C min^{-1}, and then held at temperature for 4 hours before being allowed to cool, whereupon the samples were collected, weighed, and ground with a pestle and mortar to obtain the oxides. The yield was determined by calculating the percentage conversion of cerium from the starting material to the oxide.

2.3 Methods

Scanning electron microscopy (SEM) images for ceria were collected using a Jeol JSM-7900F field emission scanning electron microscope with 5 kV acceleration voltage and magnification ranging from 1000×–30 000×. The images presented in the paper (ESI Fig. S1, S3 and S5†) were collected at a magnification of 10 000× or 20 000×. Transmission electron microscope (TEM) images of ceria were taken using a JEOL JEM-2100Plus instrument with an acceleration voltage of 200 kV and magnification ranging from 50 000×–1 500 000×. TEM images at two magnifications are presented in this paper (ESI Fig. S2†); 250 000× (Fig. S2(a)†) and 1 500 000× (Fig. S2(b)†). Powder X-

ray diffraction (PXRD) patterns were collected using a STOE STADI P instrument in transmission mode with Cu-Kα radiation ($\lambda = 1.5418$ Å). The crystallite size was calculated by applying the Scherrer equation[47] to the various diffraction peaks and taking their average with the error given by the standard deviation. The values corresponding to all reflections are shown in the ESI (Table S1† for ceria from Ce : U DES and Table S2† for ceria from Ce : U DES + 5W). N_2 adsorption analysis was conducted using an Autosorb-iQ-C from Quantachrome Anton Paar at 77 K, after degassing under vacuum at 90 °C for 1 hour followed by 200 °C for 5 hours. The BET specific surface area ($m^2\ g^{-1}$) was calculated from the adsorption branch of the isotherm, along with the micropore volume ($cm^3\ g^{-1}$) using the HK method in ASiQWin, by using Quantachrome software. Small Angle X-ray Scattering (SAXS) was performed for the ceria powders using an Anton Paar SAXSpoint 2.0 with Cu-Kα radiation ($\lambda = 1.5418$ Å) giving a q-range of $0.007\ Å^{-1} < q < 0.42\ Å^{-1}$. The data were fitted using a two-level unified power-law Beaucage function[48,49] in the NCNR SANS Analysis macros[50] in Igor Pro.[51] XPS data were acquired using a Kratos Axis SUPRA using monochromated Al-Kα (1486.69 eV) X-rays at 15 mA emission and 12 kV HT (180 W) and a spot size/analysis area of 700 × 300 μm. All data were recorded at a base pressure of below 9×10^{-9} Torr and a room temperature of 294 K. Data were analysed using CasaXPS v2.3.19PR1.0. Peaks were fit with a Shirley background prior to component analysis.

Temperature programmed reduction (TPR) profiles were collected using a Micromeritics Autochem 2920, under 20 mL min^{-1} of 5% (v/v) H_2 in argon from room temperature to 900 °C at a heating rate of 5 °C min^{-1}. In all the analyses, 50 mg of the calcined fine powder was loaded into the instrument's U-shaped quartz reactor—fixing the catalyst bed between quartz wool to hold it in place—and inserted in a temperature-controlled furnace. The sample was flushed with argon prior to analysis, to remove any traces of air. Subsequently, the gas flow was switched to the reducing atmosphere mentioned earlier while ramping the temperature up. The composition of the outlet gas was monitored using a thermal conductivity detector, and the obtained profiles were deconvoluted into constituting Gaussian peaks using "peakfit.m", a command-line peak fitting function developed in MATLAB.[52] The area underneath the peaks was integrated and the ratio of the low-temperature to high-temperature peak areas is reported as an indication of the surface-to-bulk oxygen ratio for the different samples.

CO oxidation catalytic tests were conducted using a bespoke rig that consisted of a U-shaped quartz differential reactor (4 mm internal diameter) mounted in an upstanding temperature-controlled furnace. In a typical experiment, 20 mg of ceria catalyst was dispersed in about 600 mg coarse-grained SiC (360 μm average diameter) to obtain a packed bed of 0.38 cm^3 volume. The packed bed was fixed between quartz wool. The reactant feed was composed of 3000 ppm CO and 3000 ppm of O_2 in He as the carrier gas, with a total flow rate of 300 mL min^{-1}. This gave a gas hourly space velocity (GHSV) of 2700 N mL_{CO} ($g_{catalyst}^{-1}\ h^{-1}$) (1.013 bar; 293.15 K). Immediately before coming into contact with the catalyst bed, the gas flow was passed through an inert bed of 180 mg fine SiC (53 μm; secured between quartz wool) to ensure plug flow conditions in the downstream catalyst bed. The composition of the outlet stream was analysed using an on-line non-dispersive IR gas analyser (ABB, EL3020-Uras 26). The catalytic activity was evaluated from room temperature to 500 °C, ramping up and down at 5 °C min^{-1} for at least 5 cycles to test the stability of the catalysts. The conversion (X_{CO}%) was calculated as follows to account for the change in the number of moles in the reaction:

$$X_{CO}\% = \frac{x_{CO,in} - x_{CO,out}}{x_{CO,in}(1 - 0.5 \times x_{CO,out})} \times 100 \quad (1)$$

where $x_{CO,in}$ and $x_{CO,out}$ denote the inlet and outlet CO concentrations, respectively. From the conversion data, and knowing the flow rate under normal conditions ($T = 293.15$ K and $P = 1.01325$ bar), the turnover frequencies (TOF) can be calculated using the ideal gas law as follows:

$$\mathrm{TOF}\ \left(\mathrm{mol_{CO}\ g_{catalyst}^{-1}\ min^{-1}}\right) = \frac{\frac{X_{CO}\%}{100} \times Q_{CO}\ \left(\mathrm{L\ min^{-1}}\right) \times x_{CO,in} \times 1.01325\ \mathrm{(bar)}}{0.08314\ \left(\mathrm{bar\ L\ mol^{-1}\ K^{-1}}\right) \times 293.15\ \mathrm{(K)} \times m_{catalyst}\ \mathrm{(g)}} \quad (2)$$

where Q_{CO} is the total flow rate (0.9 mL min^{-1} out of the total 300 mL min^{-1}), and $m_{catalyst}$ is the mass of the catalyst used in the experiments (typically 20 mg). Rates of reaction (as defined by the TOF) in the range $5 < X_{CO}\% < 15$ were used for the Arrhenius plots and estimating the apparent activation energies (E_a) to ensure both a negligible relative experimental error and apparent rate of reactions.

3 Results and discussion

3.1 Atom-efficient synthesis of ceria from DES

DES-based synthesis of ceria has been reported using solvothermal methods in type III DES comprising ChCl : urea[15] and by direct pyrolysis of cerium salt based type IV DES.[44] Here we demonstrate a method for the synthesis of porous ceria using a type IV DES comprising $Ce(NO_3)_3 \cdot 6H_2O$: urea in two steps: a first step whereby the homogeneous DES is heated in an oven for 24 hours at 70 °C, which leads to the solvothermal decomposition of urea resulting in the formation of cerium carbonate complexes, followed by the calcination of these complexes at 450 °C for 4 hours to obtain cerium oxide powder. During the first step, the clear DES initially turns into a cloudy suspension, which finally forms a white paste/gel. This step is analogous to the solvothermal decomposition of urea to form carbonate (CO_3^{2-}) and ammonium (NH_4^+) at a temperature of 100 °C in the ChCl : urea DES and the formation of cerium oxycarbonate ($Ce_2O(CO_3)_2$) upon the reaction of the solvated cerium ions with the carbonate ions.[15] The calcination of the white paste results in the formation of a pale yellow crystalline cerium oxide powder. The method allows for atom-efficient synthesis of cerium oxide with a ~100% yield of the cerium atom, as calculated from the percentage conversion of cerium from the starting material to the oxide.

The representative SEM and TEM images of the ceria samples produced by this method are shown in Fig. 1(a) and (b),

respectively. The images show spherical crystalline ceria particles of size ~100 nm (SEM) and crystallite size ~10 s nm (TEM). XRD patterns from the pre-calcination pastes and post-calcination powders are shown in Fig. 1(c). XRD from the pre-calcined pastes can be assigned to hexagonal cerium hydroxycarbonate ($Ce(OH)CO_3$; JCPDS 32-0189)[53] and that from the nanoparticles synthesised post calcination to the cubic phase of fluorite cerium oxide (CeO_2; JCPDS 34-0394). The formation of $Ce(OH)CO_3$ has been reported in hydrothermal synthesis techniques using millimolar solutions of cerium salts and urea or ammonium salts,[54,55] This is concordant with our synthesis, where the decomposition of urea leads to the formation of carbonate ions (CO_3^{2-}), which then react with the solvated cerium ions to produce cerium hydroxycarbonate. These $Ce(OH)CO_3$ complexes can then be calcined to produce crystalline cerium oxide.

The average crystallite size obtained from the Scherrer analysis of the XRD data is shown in Fig. 1(d) (detailed data for the various peaks are given in ESI Table S1†). The average crystallite size for the cerium oxide produced was found to be 31.4 ± 3.3 nm. This is greater than the average crystallite size obtained in the case of solvothermal synthesis of ceria from ChCl : urea[15] but is consistent with the TEM images (Fig. 1(b)) observed from the samples. Crystallite sizes for ceria are highly dependent on both the synthesis method and the calcination temperature[56–58] and comparison with hydrothermal methods with a similar calcination temperature shows crystallite sizes of up to 25 nm (ref. 57), which are similar to the values obtained here.

The two step approach facilitates the formation of micelle templated ceria by dissolving surfactants in the DES before step one and then heating the surfactant mixture to 70 °C. Heating to low temperatures allows the micelles to stay intact such that they can act as liquid crystalline templates for the synthesis of porous cerium oxide. In order to assess the capability of various surfactants as porogens, DES solutions with four cationic surfactants, C_{12}TAB, C_{16}TAB, $C_{12}TANO_3$ or $C_{16}TANO_3$, were used for the synthesis of ceria to understand the effect of both the chain length and halide in the head groups. Additionally, the non-ionic surfactant BrijC_{10} was also evaluated for comparison.‡

The representative SEM and TEM images of the ceria samples produced using DES solutions with 20% w/w surfactant are shown in ESI Fig. S1 and S2.† The addition of surfactants to the DES to produce the cerium oxide does not significantly alter the morphology of the synthesised ceria. Generally, spheroidal particles are formed in all cases; however, it appears that C_{12} chain length cationic surfactants lead to the formation of more spherical particles compared to C_{16} chain length surfactants or BrijC_{10} and C_xTANO_3 surfactants appear to induce more uniform particle shapes. This possibly arises due to the formation of uniform spherical micelles in the case of C_{12} chain length cationic surfactants,[45] whereas the longer chain length could result in more elongated micelles as is observed for C_{16} chain cationic surfactants in other DESs.[59,60]

The PXRD patterns of the ceria samples produced from Ce : U DES with added surfactants and the average crystallite size obtained from the Scherrer analysis of the XRD data for the ceria samples are shown in Fig. 1(c) and (d), respectively, alongside the ceria produced from the DES without any added surfactants (detailed data for the various peaks observed in the XRD patterns are available in ESI Table S1†). The average crystallite size for the various cerium oxides produced lies in the range 31–34 nm, which suggests that there is no change in the crystallite size due to the surfactant templating and the data are consistent with the TEM observations, which also show highly crystalline ceria powders (ESI Fig. S2†). The main differences in the surfactant templated cerium oxides arise in the porosity and catalytic oxidation of carbon monoxide and are discussed later.

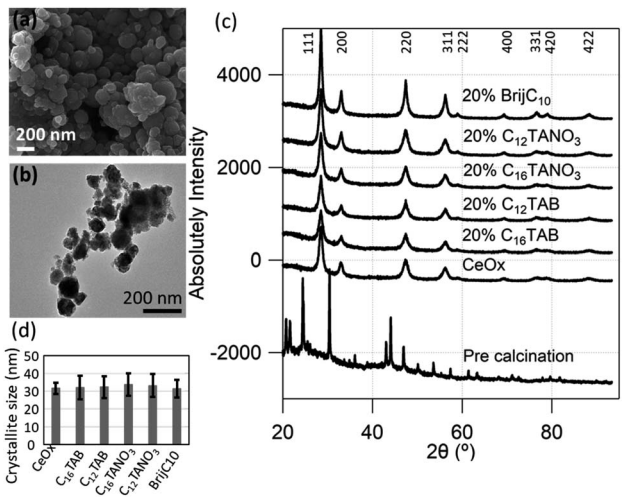

Fig. 1 (a) Representative SEM and (b) TEM images of the ceria sample made from $Ce(NO_3)_3 \cdot 6H_2O$: urea DES (Ce : U); (c) XRD patterns of representative pre-calcination ceria paste and post-calcination ceria powders, made from Ce : U DES without and with added surfactants (20% w/w); (d) mean crystallite size of the calcined ceria samples as determined by Scherrer analysis of the XRD data.

3.2 Ceria synthesised from DES without added water

Table 1 summarises the key results of the structural characterisation and catalytic tests performed on different ceria samples synthesised from Ce : U DES with and without added surfactants (20% w/w).

Fig. 2 shows the data obtained from porosity characterization of the ceria samples synthesised from Ce : U DES; Fig. 2(a) shows the N_2 adsorption/desorption isotherms and Fig. 2(b) shows the SAXS patterns from the ceria samples. The BET surface area for the ceria produced from Ce : U DES without any added surfactants was found to be 46.6 $m^2\ g^{-1}$ and the micropore volume to be 0.017 $m^2\ g^{-1}$. The surface area of the ceria synthesised here lies in the range of values reported in the literature for ceria synthesised using solvo/hydrothermal methods without any additives (10–60 $m^2\ g^{-1}$)[23,56,61–63] and is

‡ Anionic surfactants were not studied in this work as they form highly elongated micelles, which result in extremely viscous liquids at concentrations as low as 1% w/w making them difficult to handle.[45]

Table 1 Summary of the main structural and catalytic characterisation results on different ceria samples

Sample	CeO_x	+20% C_{16}TAB	+20% C_{12}TAB	+20% BrijC_{10}	+20% C_{12}TANO_3	+20% C_{16}TANO_3
BET specific surface area (m^2 g^{-1})	46.6	134.3	114.1	87.9	121.8	126.6
Micropore volume (N_2 adsorption; cm^3 g^{-1})[a]	0.017	0.053	0.045	0.036	0.05	0.05
Pore radius (SAXS; ±0.1 nm)	2.4	3.1	2.7	2.7	2.5	2.7
Ratio of surface-to-bulk oxygen peak areas (TPR)	0.33	0.54	0.46	0.45	0.49	0.48
E_a – CO oxidation (kJ mol^{-1})[b]	91.1 ± 1.8	95.8 ± 2.0	97.2 ± 1.9	86.9 ± 2.2	66.7 ± 1.1	82.6 ± 1.1
Lowest active temperature (°C)	320	345	350	310	180	265

[a] Calculated from the adsorption isotherm using the HK method. [b] Apparent activation energy ± 95% confidence bounds estimated from at least 6 measurements.

again highly dependent on the calcination temperature, with the BET surface area decreasing as the calcination temperature increases.[56] The addition of surfactants to the DES increases the porosity of the ceria synthesised. The BET surface area and the micropore volume for the templated ceria are summarised in Table 1. The results show that cationic surfactants are more effective in increasing the porosity compared to the non-ionic surfactant and longer chain length cationic surfactants result in the highest surface area; the highest BET surface area for templated ceria (134.3 m^2 g^{-1} for C_{16}TAB) is 3× the value obtained for non-templated ceria (46.6 m^2 g^{-1}) and the micropore volume for C_{16}TAB templated ceria (0.053 cm^3 g^{-1}) is three times that of non-templated ceria (0.017 cm^3 g^{-1}), a similar effect to that observed for hydrothermal synthesis of ceria with surfactant templating.[23,61,64] This is consistent with our TEM images, which show micropores between the ceria crystals along with mesopores arising from the surfactant templating.

An independent and more accurate measure of the mesopore sizes can be provided by fitting the SAXS data measured from the ceria powders. A two-level unified power-law Beaucage function was used as the fit model: the first level accounts for the scattering from the bulk powder and can be fitted to a simple power law with exponent ∼ −4 representative of Porod type scattering, and the second level details the scattering from the porous structure and was fitted to a Guinier radius (pore radius) along with a power law. The values of the pore radius obtained from the fits are given in Table 1 and show a clear variation with the surfactant used for templating. The pore radius for C_{12}TAB (2.7 ± 0.1 nm) and C_{12}TANO_3 (2.5 ± 0.1 nm) is consistent with the micelle sizes for the corresponding surfactants in Ce : U, 2.4 ± 0.2 nm for C_{12}TAB and 2.2 ± 0.2 nm for C_{12}TANO_3, and the pore radius for BrijC_{10} (2.7 ± 0.1 nm) agrees well with the micelle size of $C_{16}EO_8$ in Ce : U (3.1 ± 0.3 nm).[45] This indicates that the pores are surfactant micelle templated.

The TPR data (Fig. 3) show that all the samples exhibit two broad peaks: the first peak between 200 and 500 °C and the second above 530 °C. From the literature, the low-temperature peak is related to the reduction of surface oxygen, while the high-temperature peak corresponds to the hydrogen consumption by the lattice oxygen.[65] In particular, the reduction of ceria proceeds in two steps. Firstly, the more readily reducible surface oxygen reacts with H_2 to produce water. In the second step, sufficient thermal energy at higher temperatures enables the lattice oxygen to migrate to the surface and react with H_2, identical to the first step.[65,66] Each peak comprises two or three

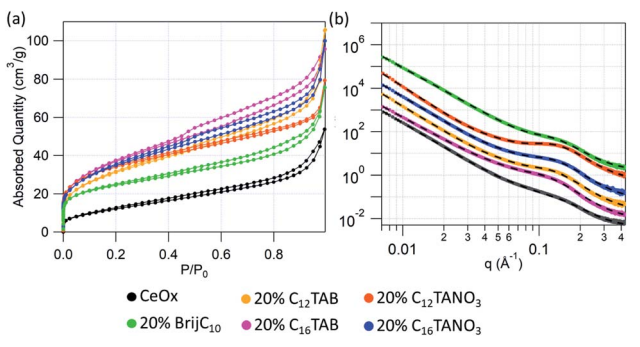

Fig. 2 (a) N_2 adsorption/desorption isotherms at 77 K of ceria samples made from Ce : U DES with and without added surfactants, demonstrating the effect of surfactants on the porosity of the materials; (b) SAXS patterns from the ceria samples fitted to a two-level unified power-law Beaucage function (black dashed lines).

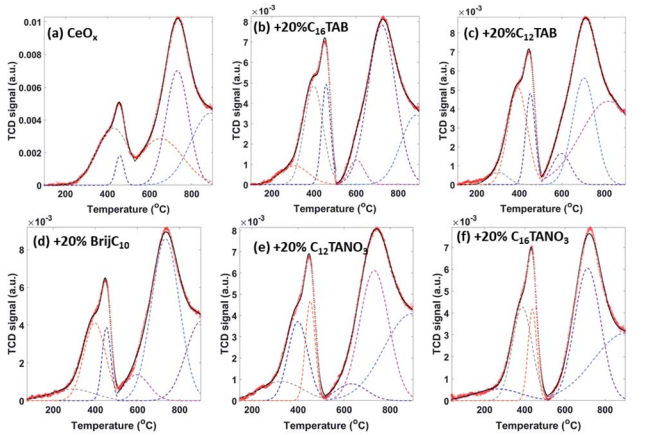

Fig. 3 Temperature-programmed reduction data for different ceria samples synthesised from the Ce : U DES (red circles) along with the respective theoretical fits obtained by linear combinations of Gaussian peaks. The individual Gaussian peaks are shown by colourful dashed lines, while the overall TPR fits are the solid black lines. The CeO_2 samples were synthesised (a) without added surfactant, (b–f) with 20% w/w surfactant, as indicated in the figure.

overlapping Gaussian peaks, as can be seen in Fig. 3. Specifically, the presence of a ubiquitous shoulder around 400 °C signifies the presence of different types of surface oxygen, with variable propensities to reduction.[67] Integrating the areas underneath the low and high temperature peaks and calculating their ratio provides an estimation of the relative abundances of the surface to bulk oxygen moieties.[13] These results are summarised in Table 1 and they clearly show that all the surfactant-templated samples are more reducible than the surfactant-free ceria, possessing higher proportions of surface-to-bulk oxygen; 0.54 for C_{16}TAB templated ceria as compared to 0.33 for non-templated ceria.

Fig. 4 presents the results of the catalytic CO oxidation activity of the different materials, serving as a model reaction for comparing the activity of different samples. As can be seen in Fig. 4(a), contrary to what is anticipated from the TPR results, not all the surfactant-assisted synthesis routes yield catalysts more active than the surfactant-free approach. In fact, while nitrate-containing surfactants produce ceria of much superior catalytic activity (compared to surfactant-free synthesis), the halide-containing ones yield catalysts that are less active than the product of the surfactant-free route despite their higher porosity and surface area. Specifically, the former samples are already active at temperatures as low as 180 °C (for $C_{12}TANO_3$) and 265 °C (for $C_{16}TANO_3$), while the latter samples only start to show activity at 345–350 °C (for C_{16}TAB and C_{12}TAB; Table 1). Along the same lines, the CeO_x synthesised using nitrate containing surfactants achieve CO conversions in excess of 85% at 500 °C, as compared to values below 40% for the CeO_x synthesised using bromide containing surfactants (Fig. 4(a)). Surprisingly, the ceria produced by adding 20% C_{16}TAB has both the greatest surface area and the highest surface-to-bulk oxygen ratio (Table 1). These observations are in agreement with the literature as it is well known that halides poison the catalysts by chemically bonding to the active sites on the CeO_x catalyst.[68,69] Therefore, this mechanism of deactivation can be avoided by employing halide-free surfactants. Concerning the CeO_x synthesised using BrijC_{10}, it is slightly more active than CeO_x from surfactant free synthesis, yet much less active than those synthesised using nitrate-based surfactants. This can be understood in the light of its intermediate specific surface area and surface-to-bulk oxygen content.

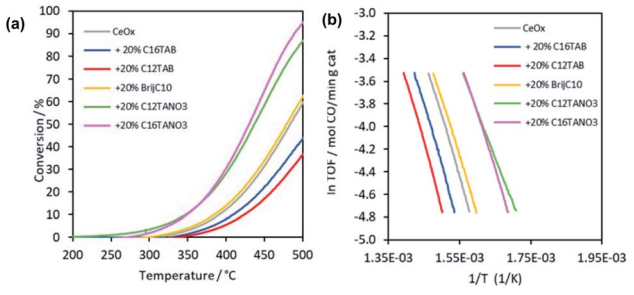

Fig. 4 (a) Activity of different ceria samples made from Ce : U DES in the catalytic oxidation of CO presented in terms of reactant conversion and the corresponding turnover frequencies. (b) Arrhenius plots based on the data of conversions in the range of 5–15%.

One must exercise caution when comparing the relative activities of different samples based on conversion as the value is extremely dependent on the experimental conditions (especially space velocity). Instead, the apparent rate of reactions (defined as the TOF) calculated from low conversion data (<15%) is reported. These values are used in the Arrhenius plot (Fig. 4(b) to estimate apparent activation energies providing a more reliable and robust basis for comparing the intrinsic activity of different catalysts. We also note that this is possible thanks to the differential configuration of our reactor to ensure no interference from mass and/or heat transfer limitations.[70] From these plots, we calculated the apparent activation energies (E_a) for the catalytic oxidation of CO with different samples. The results (summarised in Table 1) are consistent with activity trends mentioned earlier, with C_{16}TAB and C_{12}TAB-based products showing the highest values. More importantly, $C_{12}TANO_3$-based ceria shows E_a as low as 66.7 ± 1.1 kJ mol^{-1}, which is among the lowest in the literature.[12,71,72] Such low apparent activation energy makes this material an attractive candidate for further examination in application areas like low-temperature CO oxidation and exhaust emission control.

XPS and SEM EDX measurements on the calcined CeO_x samples indicate the presence of carbon in all samples, including in CeO_x made without any added surfactants. The carbon in CeO_x is likely to arise from the urea in the DES used for the synthesis. No explicit trend in the carbon content was noticed between the different CeO_x samples, made from the DES with or without added surfactants, and the overall carbon content between the samples remains similar. This indicates that while there is some carbon present in all the samples, the trends observed in the catalytic activity of CeO_x are not influenced by it as carbon is present in similar quantities in all samples, including the ceria made from DES without any added surfactants.

XPS measurements show the surface composition of the calcined ceria samples to be made up of cerium, oxygen and carbon atoms, with both Ce^{3+} and Ce^{4+} valence states present for the cerium. The relative abundance of Ce^{3+} is 12–20% of the total cerium concentration. From the literature, it can be expected that the specific rate of the reaction, an indicator of the activity, will increase with the Ce^{3+} fraction in the samples.[58] However, this trend is not observed for our ceria samples as the activity is dominated by the increase in the surface area for surfactant templated ceria compared to non-templated ceria, *i.e.* for the BrijC_{10} and CTANO_3 templated ceria samples. For the case of the C_{12}TAB and C_{16}TAB templated ceria, halide poisoning of the catalytic sites is a more important effect. The XPS data along with a more detailed discussion are presented in the ESI.†

3.3 Ceria synthesised from DES with added water

The same method, as used for the synthesis of ceria from the Ce : U DES, can be applied whereby water is added to change the morphology/porosity. Water is known to affect the DES nanostructure by disrupting the H-bonding network in the solvents,[73–75] which in turn can alter particle growth and the

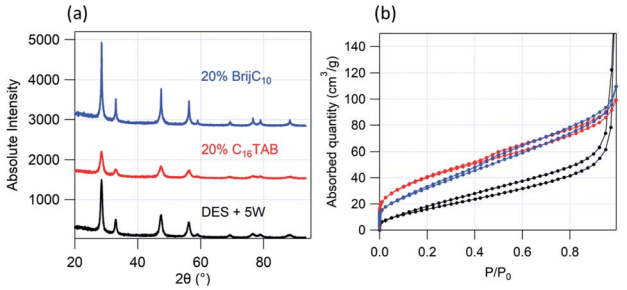

Fig. 5 (a) XRD patterns of ceria samples made from Ce : U DES with water (molar ratio 1 : 5) and added surfactants (20% w/w) after calcination; (b) N_2 adsorption/desorption isotherms at 77 K for the corresponding samples.

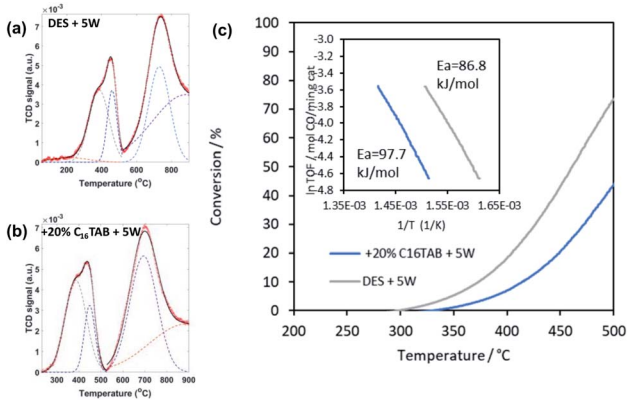

Fig. 6 (a and b) TPR data and peak deconvolution results for the ceria samples prepared from Ce : U DES with added water, molar ratio 1 : 5; (c) CO oxidation activity of ceria samples prepared from DES with added water as a function of temperature. The inset shows the corresponding Arrhenius plots using conversion data in the range of 5–15%.

morphology in solvothermal synthesis.[15,29] In this case, water or water along with 20% w/w surfactants was added to the DES before heating (step one). The solutions with water (and surfactants) were then heated in an oven at 70 °C and thereafter the pastes obtained are calcined at 450 °C to obtain ceria powders.

SEM images from ceria powder synthesised from DES : water in a molar ratio of 1 : 5 (DES + 5W) and DES + 5W with 20% w/w C_{16}TAB or BrijC_{10} are shown in ESI Fig. S3.† Ceria made from DES + 5W shows some morphological differences compared to ceria synthesised from DES without water; spindle shaped particles are observed in the case of DES + 5W compared to spheroidal particles observed in the case of synthesis without water. A similar effect is observed for the synthesis of ceria in ChCl : urea DES,[15] where water induces directional growth of cerium oxide due to the presence of hydroxyl groups limiting lateral growth resulting in 1D structures. In the case of synthesis from DES + 5W with surfactants, the surfactants can also interact with the surface of the growing particles, influencing the morphology of the ceria produced; spheroidal ceria particles similar to those obtained from syntheses from Ce : U DES with surfactants without added water are observed. The PXRD data are shown in Fig. 5(a) and the calculated crystallite sizes are summarised in Table S2.† No major changes in the average crystallite sizes are observed when using DES + 5W (30.5 ± 7.2 nm) or 5W + surfactants (30.2 ± 6.6 nm for 5W + C_{16}TAB, 32.3 ± 8.2 nm for 5W + C_{12}TAB and 35.3 ± 3.9 nm for 5W + BrijC_{10}), suggesting that the crystallinity is determined by the synthesis method and the calcination temperature and not by additives. However, some small changes are observed in the case of porosity and CO oxidation activity.

Fig. 5(b) shows the N_2 adsorption/desorption isotherms for the ceria samples synthesised from Ce : U DES with water (DES + 5W) and added surfactants (20% w/w). The BET specific surface area of ceria synthesised from DES + 5W was found to be 68.8 $m^2\ g^{-1}$ and the micropore volume was calculated to be 0.022 $cm^3\ g^{-1}$. This indicates a higher porosity and surface area when compared to ceria synthesised with DES without added water (BET surface area 46.6 $m^2\ g^{-1}$ and micropore volume 0.017 $cm^3\ g^{-1}$). The surface area obtained here is comparable to the solvothermal synthesis of highly elongated ceria nanorods in ChCl : urea DES with water, where both the morphology and microporosity of the ceria synthesised depends on the molar ratio of DES : water;[15] a BET surface area of ~75 $m^2\ g^{-1}$ was reported for a DES : water molar ratio of 1 : 10. Samples made from DES + 5W with added surfactants also show a slight increase in the BET surface area (~10%); the BET surface area for ceria made from DES + 5W + C_{16}TAB is 148.1 $m^2\ g^{-1}$ compared to 134.3 $m^2\ g^{-1}$ for ceria synthesised from DES + C_{16}TAB and for DES + 5W + BrijC_{10}, the BET surface area is 130.1 $m^2\ g^{-1}$ compared to 87.9 $m^2\ g^{-1}$ for DES + BrijC_{10}.

Fig. 6 summarises the TPR data (Fig. 6(a) and (b)) and the results of catalytic tests (Fig. 6(c)) on two samples synthesised from DES + 5W and DES + 5W + C_{16}TAB. The addition of water made the product of surfactant-free synthesis more reducible (giving a higher ratio of surface to bulk oxygen, 0.44, compared to 0.33 in the synthesis without added water) along with slightly increasing its surface area and porosity. As a result, water addition yielded a product that was more active in oxidising CO, showing a lower apparent activation energy of 86.8 ± 1.7 kJ mol^{-1} (compared to 91.1 ± 1.8 kJ mol^{-1} when made from DES without added water). In contrast, adding water to the synthesis in the presence of C_{16}TAB made the product less reducible (surface to bulk oxygen = 0.47) and less active in CO oxidation (E_a = 97.7 ± 1.8 kJ mol^{-1}). In particular, the addition of water appears to promote the incorporation of the surfactant and/or its residual halide into the ceria product, giving rise to its inferior catalytic activity.

4 Conclusions

We demonstrate a green route to the synthesis of high surface-area, mesoporous, crystalline ceria by employing a novel deep eutectic solvent, wherein cerium acts both as a reactant and a constituent of the solvent medium. This is one of the less intensive synthetic routes through which ceria structures of these sizes have been achieved, making this DES-solvothermal

method with a particularly mild set of conditions highly attractive for the manufacturing of this type of nanomaterial, using novel metal salt based solvents, with a 100% cerium yield. In principle the solvothermal method described here can be extended to the synthesis of other metal oxides from metal salts that are capable of forming type IV DES.

We show that the surface area and catalytic activity of the ceria can be altered, generally enhanced, by surfactant templating using DES solutions containing cationic and non-ionic surfactants. Halide-free cationic surfactants $C_{12}TANO_3$ and $C_{16}TANO_3$ are presented as superior choices for increasing the surface area of ceria, while avoiding halide poisoning in the catalytic oxidation of CO to CO_2. In particular, the ceria synthesised in the presence of 20% $C_{12}TANO_3$ is already active at temperatures as low as 180 °C. This translates into one of the lowest apparent activation energies reported in the literature for bare ceria powders (66.7 ± 1.1 kJ mol^{-1}), warranting its further investigation for various industrial applications such as in the manufacturing of automotive three-way catalysts.

Data availability

The data that support the findings of this study are openly available in the Bath research data archive system at **https://doi.org/10.15125/BATH-01190**.

Conflicts of interest

The authors declare no conflicts of interest.

Acknowledgements

The authors acknowledge funding from EPSRC (Grant Number EP/S020772/1 & Grant Number EP/S021019/1). We thank Dr Gabriele Kociok-Köhn for her help with the acquisition of PXRD data and Dr Philip Fletcher for his assistance in the SEM and TEM data measurement. The X-ray photoelectron (XPS) data collection was performed at the EPSRC National Facility for XPS ("HarwellXPS"), operated by Cardiff University and UCL, under Contract No. PR16195. The data that support the findings of this study are openly available in the Bath research data archive system at **https://doi.org/10.15125/BATH-001190**.

Notes and references

1 A. Trovarelli, *Catal. Rev.*, 1996, **38**, 439–520.
2 J. Kašpar, P. Fornasiero and M. Graziani, *Catal. Today*, 1999, **50**, 285–298.
3 M. Stoukides, *Catal. Rev.*, 2000, **42**, 1–70.
4 X. Yin, L. Hong and Z.-L. Liu, *J. Membr. Sci.*, 2006, **268**, 2–12.
5 I. Porqueras, C. Person, C. Corbella, M. Vives, A. Pinyol and E. Bertran, *Solid State Ionics*, 2003, **165**, 131–137.
6 A. Azens, L. Kullman, D. D. Ragan, C. G. Granqvist, B. Hjörvarsson and G. Vaivars, *Appl. Phys. Lett.*, 1996, **68**, 3701–3703.
7 N. Özer, *Sol. Energy Mater. Sol. Cells*, 2001, **68**, 391–400.
8 T. Montini, M. Melchionna, M. Monai and P. Fornasiero, *Chem. Rev.*, 2016, **116**, 5987–6041.
9 S. Datta and L. Torrente-Murciano, *Curr. Opin. Chem. Eng.*, 2018, **20**, 99–106.
10 H. J. Kim, M. G. Jang, D. Shin and J. W. Han, *ChemCatChem*, 2020, **12**, 11–26.
11 L. Torrente-Murciano and F. Garcia-Garcia, *Catal. Commun.*, 2015, **71**, 1–6.
12 E. Aneggi, J. Llorca, M. Boaro and A. Trovarelli, *J. Catal.*, 2005, **234**, 88–95.
13 S. C. Rood, H. B. Ahmet, A. Gomez-Ramon, L. Torrente-Murciano, T. R. Reina and S. Eslava, *Appl. Catal., B*, 2019, **242**, 358–368.
14 L. Torrente-Murciano, A. Gilbank, B. Puertolas, T. Garcia, B. Solsona and D. Chadwick, *Appl. Catal., B*, 2013, **132**, 116–122.
15 O. S. Hammond, K. J. Edler, D. T. Bowron and L. Torrente-Murciano, *Nat. Commun.*, 2017, **8**, 1–7.
16 R. Lenka, T. Mahata, P. Sinha and A. Tyagi, *J. Alloys Compd.*, 2008, **466**, 326–329.
17 C.-C. Hwang, T.-H. Huang, J.-S. Tsai, C.-S. Lin and C.-H. Peng, *Mater. Sci. Eng., B*, 2006, **132**, 229–238.
18 E. Novitskaya, J. P. Kelly, S. Bhaduri and O. A. Graeve, *Int. Mater. Rev.*, 2021, **66**, 188–214.
19 X. Li, F. Chen, X. Lu, C. Ni and Z. Chen, *J. Rare Earths*, 2009, **27**, 943–947.
20 M. Lundberg, H.-J. Wang, P. Blennow and M. Menon, *Ceram. Int.*, 2011, **37**, 797–802.
21 C. Sun, H. Li and L. Chen, *Energy Environ. Sci.*, 2012, **5**, 8475–8505.
22 D. Zhang, X. Du, L. Shi and R. Gao, *Dalton Trans.*, 2012, **41**, 14455–14475.
23 A. Bumajdad, J. Eastoe and A. Mathew, *Adv. Colloid Interface Sci.*, 2009, **147–148**, 56–66.
24 D. M. Lyons, K. M. Ryan and M. A. Morris, *J. Mater. Chem.*, 2002, **12**, 1207–1212.
25 P. Paschalidou and C. R. Theocharis, *RSC Adv.*, 2019, **9**, 7025–7031.
26 D. Gu and F. Schüth, *Chem. Soc. Rev.*, 2014, **43**, 313–344.
27 R. I. Walton, *Prog. Cryst. Growth Charact. Mater.*, 2011, **57**, 93–108.
28 E. L. Smith, A. P. Abbott and K. S. Ryder, *Chem. Rev.*, 2014, **114**, 11060–11082.
29 O. S. Hammond, S. Eslava, A. J. Smith, J. Zhang and K. J. Edler, *J. Mater. Chem. A*, 2017, **5**, 16189–16199.
30 H.-G. Liao, Y.-X. Jiang, Z.-Y. Zhou, S.-P. Chen and S.-G. Sun, *Angew. Chem., Int. Ed.*, 2008, **47**, 9100–9103.
31 L. Hu, Z. Yan, J. Zhang, X. Peng, X. Mo, A. Wang and L. Chen, *J. Mater. Sci.*, 2019, **54**, 11009–11023.
32 A. P. Abbott, J. C. Barron, G. Frisch, K. S. Ryder and A. F. Silva, *Electrochim. Acta*, 2011, **56**, 5272–5279.
33 A. P. Abbott, K. E. Ttaib, G. Frisch, K. S. Ryder and D. Weston, *Phys. Chem. Chem. Phys.*, 2012, **14**, 2443–2449.
34 P. Sebastian, M. I. Giannotti, E. Gómez and J. M. Feliu, *ACS Appl. Energy Mater.*, 2018, **1**, 1016–1028.
35 M. Wang, S. Fang and X. Liang, *J. Pharm. Biomed. Anal.*, 2018, **158**, 262–268.

36 S. N. Pedro, M. G. Freire, C. S. R. Freire and A. J. D. Silvestre, *Expert Opin. Drug Delivery*, 2019, **16**, 497–506.
37 J. Jiang, C. Yan, X. Zhao, H. Luo, Z. Xue and T. Mu, *Green Chem.*, 2017, **19**, 3023–3031.
38 E. R. Cooper, C. D. Andrews, P. S. Wheatley, P. B. Webb, P. Wormald and R. E. Morris, *Nature*, 2004, **430**, 1012–1016.
39 E. R. Parnham, E. A. Drylie, P. S. Wheatley, A. M. Slawin and R. E. Morris, *Angew. Chem.*, 2006, **118**, 5084–5088.
40 R. E. Morris, *Chem. Commun.*, 2009, 2990–2998.
41 F. Himeur, I. Stein, D. S. Wragg, A. M. Slawin, P. Lightfoot and R. E. Morris, *Solid State Sci.*, 2010, **12**, 418–421.
42 R. A. Maia, B. Louis and S. A. Baudron, *CrystEngComm*, 2021, **23**, 5016–5032.
43 A. J. Exposito, P. J. Barrie and L. Torrente-Murciano, *ACS Sustainable Chem. Eng.*, 2020, **8**, 18297–18302.
44 O. S. Hammond, D. T. Bowron and K. J. Edler, *ACS Sustainable Chem. Eng.*, 2019, **7**, 4932–4940.
45 I. Manasi, M. R. Andalibi, R. S. Atri, J. Hooton, S. M. King and K. J. Edler, *J. Chem. Phys.*, 2021, **155**, 084902.
46 M. Nyden and O. Söderman, *Langmuir*, 1995, **11**, 1537–1545.
47 P. Scherrer, in *Bestimmung der inneren Struktur und der Größe von Kolloidteilchen mittels Röntgenstrahlen*, Springer Berlin Heidelberg, Berlin, Heidelberg, 1912, pp. 387–409.
48 G. Beaucage, *J. Appl. Crystallogr.*, 1995, **28**, 717–728.
49 G. Beaucage, *J. Appl. Crystallogr.*, 1996, **29**, 134–146.
50 S. R. Kline, *Reduction and Analysis of SANS and USANS Data Using IGOR Pro*, 2006.
51 *Igor Pro 6.3 by Wavemetrics*, **https://www.wavemetrics.com/order/order_igordownloads6.htm**.
52 T. O'Haver, *Pragmatic Introduction to Signal Processing: Applications in Scientific Measurement*, University of Maryland at College Park, 2021, pp. 373–378.
53 M. Hirano and E. Kato, *J. Mater. Sci. Lett.*, 1999, **18**, 403–405.
54 H.-C. Wang and C.-H. Lu, *Mater. Res. Bull.*, 2002, **37**, 783–792.
55 K. Nakagawa, Y. Tezuka, T. Ohshima, M. Katayama, T. Ogata, K.-I. Sotowa, M. Katoh and S. Sugiyama, *Adv. Powder Technol.*, 2016, **27**, 2128–2135.
56 M. Hirano and E. Kato, *J. Am. Ceram. Soc.*, 1999, **82**, 786–788.
57 D. Valechha, S. Lokhande, M. Klementova, J. Subrt, S. Rayalu and N. Labhsetwar, *J. Mater. Chem.*, 2011, **21**, 3718–3725.
58 J. M. López, A. L. Gilbank, T. García, B. Solsona, S. Agouram and L. Torrente-Murciano, *Appl. Catal., B*, 2015, **174–175**, 403–412.
59 A. Sanchez-Fernandez, T. Arnold, A. J. Jackson, S. L. Fussell, R. K. Heenan, R. A. Campbell and K. J. Edler, *Phys. Chem. Chem. Phys.*, 2016, **18**, 33240–33249.
60 R. S. Atri, A. Sanchez-Fernandez, O. S. Hammond, I. Manasi, J. Doutch, J. P. Tellam and K. J. Edler, *J. Phys. Chem. B*, 2020, **124**, 6004–6014.
61 N. Laosiripojana, W. Sutthisripok and S. Assabumrungrat, *Chem. Eng. J.*, 2007, **127**, 31–38.
62 A. Tok, S. Du, F. Boey and W. Chong, *Mater. Sci. Eng., A*, 2007, **466**, 223–229.
63 M. Piumetti, S. Bensaid, T. Andana, M. Dosa, C. Novara, F. Giorgis, N. Russo and D. Fino, *Catalysts*, 2017, **7**, 174.
64 D. Terribile, A. Trovarelli, J. Llorca, C. de Leitenburg and G. Dolcetti, *J. Catal.*, 1998, **178**, 299–308.
65 M. Boaro, M. Vicario, C. de Leitenburg, G. Dolcetti and A. Trovarelli, *Catal. Today*, 2003, **77**, 407–417.
66 F. Giordano, A. Trovarelli, C. de Leitenburg and M. Giona, *J. Catal.*, 2000, **193**, 273–282.
67 M. Piumetti, S. Bensaid, N. Russo and D. Fino, *Appl. Catal., B*, 2015, **165**, 742–751.
68 S. Dey and G. C. Dhal, *Mater. Sci. Energy Technol.*, 2020, **3**, 6–24.
69 M. Hammes, K. Stöwe and W. F. Maier, *Appl. Catal., B*, 2012, **117–118**, 397–405.
70 F. Kapteijn and J. A.Moulijn, Laboratory Catalytic Reactors: Aspects of Catalyst Testing, in *Handbook of Heterogeneous Catalysis*, ed. G. Ertl, H. Knözinger, F. Schüth and J. Weitkamp, Wiley-VCH, Weinheim, 2nd edn, 2008, pp. 2019–2045.
71 H. Freund, G. Meijer, M. Scheffler, R. Schlögl and M. Wolf, *Angew. Chem., Int. Ed.*, 2011, **50**, 10064–10094.
72 S. Rood, PhD thesis, University of Bath, 2019.
73 I. Manasi, S. J. Bryant, O. S. Hammond and K. J. Edler, *Eutectic Solvents and Stress in Plants*, Academic Press, 2021, vol. 97, pp. 41–68.
74 M. Roldán-Ruiz, R. Jiménez-Riobóo, M. Gutiérrez, M. Ferrer and F. del Monte, *J. Mol. Liq.*, 2019, **284**, 175–181.
75 O. S. Hammond, D. T. Bowron and K. J. Edler, *Angew. Chem., Int. Ed.*, 2017, **56**, 9782–9785.

